J. Fluid Mech. (1981), *vol.* 105, *pp.* 157–176
Printed in Great Britain

Steady draw-down of a liquid jet under surface tension and gravity

By D. B. BOGY

Department of Mechanical Engineering, University of California, Berkeley

(Received 3 July 1979 and in revised form 25 March 1980)

When a water tap is turned off gradually, a critical point is reached at which the flow changes abruptly from a continuous stream to a series of drops that form at the tap. This problem is studied within the context of a one-dimensional (Cosserat) jet theory. The exact inviscid, steady, nonlinear jet equations are solved and steady draw-down shapes are obtained for various values of Weber and Bond numbers. A critical Weber number is obtained (as a function of Bond number) below which no steady solution is found that satisfies the constraints imposed at the nozzle. The results are compared with classical experiments and appear to explain the observed 'first critical velocity'.

1. Introduction

The phenomenon to be investigated can be observed with a household water tap. At a very low rate of flow a steady laminar stream runs from the tap and its radius is seen to decrease with distance from the tap. Of course this 'steady' stream is unstable and small disturbances grow along its length so that it breaks up into drops 10 or 15 cm from the tap according to Rayleigh's (1879) theory. If the flow rate is reduced gradually by turning off the faucet slowly, the continuous portion of the stream decreases to maybe 3 or 4 cm and then abruptly disappears altogether so that the stream forms drops at the tap.

A slightly more controlled but simple experiment illustrates the phenomenon better. A wine bottle half filled with water and fitted with a rubber stopper that holds a glass capillary tube gives such a stream when turned upside down. As the water drains out the pressure inside the bottle gradually decreases, causing a very gradual reduction in flow rate. When some critical condition is reached the abrupt cut-off occurs.

The Rayleigh stability phenomenon is well understood and is not the main topic of interest here. Instead we seek to predict the steady draw-down shape and the cut-off condition just described. The cut-off condition is important in many industrial applications. Some processes such as ink-jet printing depend on having a steady stream, the break-up of which can be controlled. Other processes need to have drops forming at the nozzle and the maximum flow rate for which this is possible is of interest.

This problem was studied experimentally by Smith & Moss (1917) and Tyler & Richardson (1925). These experiments of jets emanating from nozzles differed from those of Savart (1833), where the jets were formed by a hole in the bottom of a tank. Figure 10 is reproduced from Smith & Moss and shows the length of the continuous portion of the jet as a function of head (or velocity at the nozzle) for various diameter

nozzles. The fluid is mercury and it is discharging into a solution of $HgNO_3$. It was determined by Smith & Moss that a portion of the segments BC of all the curves would coincide and form a straight line, which if extended from B would pass through the origin, if length/diameter is plotted against $V(\rho d/\sigma)^{\frac{1}{2}}$ (where ρ = density, d = diameter, σ = surface tension). Figure 11, taken from Tyler & Richardson, shows such a plot for various liquids discharging into air through various size nozzles. These experiments will not be discussed in detail at this point. Suffice it to say here it was determined that the maximum, designated as the 'second critical point', occurs at the onset of turbulence, and the part of the curve beyond the maximum is controlled primarily by viscosity. In the straight portion surface tension was found to dominate, and the kink at the low end, designated as the 'first critical point', was not explained.

Other experiments have been reported but most have been concerned primarily with high-velocity jets and viscous effects. Scriven & Pigford (1959) measured the draw-down shapes of a jet for two values of the Weber number. They also assumed an exit profile and used mass and momentum balance in conjunction with boundary-layer theory and the free-fall equation to derive a simple approximate expression for the draw-down shape. Middleman & Gavis (1961) studied experimentally the contraction of jets, neglecting gravity. They recorded the ratio of final diameter to initial diameter and found that for high viscosity the Newtonian jets actually expand rather than contract. They used integral methods to derive a relation for the dependence of the final diameter on the Reynolds and Weber number. Their relation reduces to the high-velocity, low-viscosity result, $\frac{1}{2}\sqrt{3}$, of Harmon (1955) in those limits.

Duda & Vrentas (1967) presented an analysis of the draw-down problem in which they used a non-orthogonal co-ordinate system with one co-ordinate surface coinciding with the jet surface. The equations of motion in that co-ordinate system were solved by finite differences for the shape of the jet. Lienhard (1968) considered the steady draw-down problem by methods similar to those used by Scriven & Pigford. He obtained some draw-down shapes but they were restricted to high Weber numbers. Goren & Wronski (1966) studied the shape of low-speed capillary jets with gravity neglected by two theoretical approaches. One was a perturbation analysis about the final state and the other was a boundary-layer analysis near the point of jet formation. They were concerned primarily with viscous effects, much along the same lines as Middleman & Gavis. Finally Scheele & Meister (1968) considered the injection of one Newtonian liquid into a second stationary immiscible liquid. Using simple force balance arguments they derived an expression for the critical velocity for jet formation. They compared their result with several experiments and obtained acceptable agreement in most cases.

The approach here is entirely different from those in the investigations just cited. A one-dimensional theory is used, the derivation of which rests on a fluid line with directors (called a Cosserat continuum). The development of the general theory can be found in Green, Naghdi & Wenner (1974), and the specialization to a straight circular jet is given in Green (1976). The theory has been applied to several jet problems with considerable success. See, for example, Bogy (1978, 1979*a*, *b*), where the spatial stability and drop formation of circular jets emanating from a nozzle are studied. Also see Caulk & Naghdi (1979*a*, *b*) who deal with the stability and effects of rotation of elliptical viscous jets. Finally, Naghdi (1979) has presented such a theory for Newtonian and non-Newtonian jets and he used it to represent Poiseuille flow in a

pipe. A discussion of the derivation of the Cosserat jet theory is beyond the scope of this paper. Readers who are unfamiliar with this approach can find the complete theoretical development as well as applications to particular problems in the literature just cited.

In §2 the inviscid form of the equations are recorded in dimensionless form and the problem is formulated. Then a constraint on the conditions at the nozzle is derived from a first integral.

In §3 a single nonlinear ordinary differential equation is obtained for the jet radius. This equation is integrated once and cast in terms of arc length variables on the jet surface. In §4 a scheme is developed for integrating this equation to obtain the draw-down shape. In §5 the equations are linearized and a closed-form solution is derived. The results are compared with those of the nonlinear theory.

In §6 the results are compared with the classical experiments of Smith & Moss (1917) and Tyler & Richardson (1925), and a discussion is given in §7.

2. Straight circular jet equations and problem formulation

The Cosserat jet equations for a straight circular jet centred on the z axis which points vertically downward were given in Green (1976). In dimensionless form the inviscid equations (equations (6.9)–(6.14) of Green, with $\eta = 1$ and $R = \infty$) appear as

$$(\phi^2)_t + (v\phi^2)_z = 0, \quad v_z + 2u = 0, \tag{2.1, 2.2}$$

$$\phi^2(v_t + vv_z) = -q_z + \frac{2}{W}\left[\frac{\phi}{(1+\phi_z^2)^{\frac{1}{2}}}\right]_z + \frac{\phi^2}{F}, \tag{2.3}$$

$$\tfrac{1}{4}\phi^4(u_t + vu_z + u^2) = q - \frac{1}{W}\left[\frac{\phi}{(1+\phi_z^2)^{\frac{1}{2}}} - \frac{\phi^2\phi_{zz}}{(1+\phi_z^2)^{\frac{3}{2}}}\right], \tag{2.4}$$

$$q = p - p_0\phi^2, \quad n_3 = -q - p_0\phi^2, \tag{2.5}$$

where $\phi(z,t)$, $v(z,t)$ and $u(z,t)$ are the dimensionless jet radius, axial velocity and director velocity; p is the pressure resultant, p_0 the atmospheric pressure and n_3 is the axial component of stress resultant. The dimensionless numbers W and F are the Weber and Froude numbers defined by

$$W = \rho a v_0^2/\sigma, \quad F = v_0^2/ga, \tag{2.6}$$

in which ρ is the fluid density, a is the nozzle radius, v_0 is the jet velocity at the nozzle, σ is surface tension, and g is the acceleration of gravity. Subscripts in (1)–(5) denote partial differentiation and the quantities have been rendered dimensionless through the division of

$$z, \phi \text{ by } a; \quad t \text{ by } a/v_0; \quad v \text{ by } v_0; \quad u \text{ by } v_0/a; \quad p, q, n_3 \text{ by } \pi\rho v_0^2 a^2; \quad p_0 \text{ by } \rho v_0^2. \tag{2.7}$$

In addition to the dimensionless parameters defined in (2.6), the Bond number, B, defined as

$$B = W/F = \rho a^2 g/\sigma, \tag{2.8}$$

will occur in the solutions. This parameter is independent of velocity and is determined by the fluid, the nozzle radius, and gravity. It is positive or negative according as the

jet is flowing downward ($g > 0$) or upward ($g < 0$), i.e. a fountain. In comparing the equations given here with those in Green (1976) one should note that the latter uses σ and T for density and surface tension.

If equation (2.4) is differentiated the quantity q_z can be eliminated from the result and equation (2.3). Then with the assumption of steady flow and the use of (2.2) to eliminate u, the system (2.1)–(2.4) can be written in terms of v and ϕ as

$$v\phi^2 = 1, \tag{2.9}$$

$$vv_z - \tfrac{1}{2}\phi\phi_z(vv_{zz} - \tfrac{1}{2}v_z^2) - \tfrac{1}{8}\phi^2 vv_{zzz} = \frac{1}{W}\left[\frac{\phi_z}{\phi^2(1+\phi_z^2)^{\frac{1}{2}}} + \frac{\phi_z\phi_{zz}}{\phi(1+\phi_z^2)^{\frac{1}{2}}} + \frac{\phi_{zzz}}{(1+\phi_z^2)^{\frac{3}{2}}} - \frac{3\phi_z\phi_{zz}^2}{(1+\phi_z^2)^{\frac{5}{2}}}\right] + \frac{1}{F}. \tag{2.10}$$

We seek solutions of (2.9) and (2.10) on the semi-infinite jet region $z > 0$ which satisfy the boundary conditions

$$\phi(0) = 1, \quad v(0) = 1, \tag{2.11}$$

and

$$\phi \to 0, \quad \phi_{zz} \to 0, \quad v \to \infty \quad \text{as} \quad z \to \infty. \tag{2.12}$$

As will be seen an additional boundary condition is required at $z = 0$ in order to determine the solution uniquely. In principle this condition should be determined by the flow inside the nozzle together with certain jump conditions at the nozzle which are derivable from the conservation laws. These conditions would have to take into account surface tension on the free jet surface and some assumed interfacial energy condition inside the nozzle. Since the theory used here is not sufficiently general to apply to the flow inside the nozzle such an approach cannot be pursued. Therefore the additional condition needed at the nozzle will be based on a specific assumption which will provide a constraint that finally uniquely determines the solution obtained.

In order to derive the constraint condition at $z = 0$ we return to the steady form of (2.3). With use of (2.9), (2.3) can be integrated to yield

$$v - C = -q + \frac{2}{W}\left[\frac{\phi}{(1+\phi_z^2)^{\frac{1}{2}}}\right] + \int_0^z \frac{\phi^2}{F}\, d\zeta, \tag{2.13}$$

where C is a constant of integration. The desired condition is related to the choice of C. Evaluating (2.13) as $z \to 0^+$ we obtain

$$v^+ - C = -q^+ + \frac{2}{W}\left[\frac{\phi}{(1+\phi_z^2)^{\frac{1}{2}}}\right]^+. \tag{2.14}$$

We now choose the constant of integration C by

$$C = v^+ \tag{2.15}$$

so that (2.14) yields

$$q^+ = \frac{2}{W}\left[\frac{\phi}{(1+\phi_z^2)^{\frac{1}{2}}}\right]^+. \tag{2.16}$$

Therefore this choice of C amounts to the assumption that the net resultant axial force on the jet at the nozzle equals the pressure force p_0 plus the axial component of the surface tension force. This is in agreement with known results, based on the classical Laplace equation (see Pitts 1974), in the case of a static pendant drop. (One can easily show that the Laplace equation is recovered from (2.9) and (2.10) in the limit of zero velocity.) Equation (2.16) also gives the proper result for inviscid flow from a straight

pipe nozzle in the high velocity limit where $\phi_z^+ = 0$ is expected to apply. Indeed, it will be shown in the linearized analysis of §5 that (2.16) implies $\phi_z^+ = 0$ in the high-velocity limit.

Next we evaluate (2.4) as $z \to 0^+$ to obtain

$$q^+ = \tfrac{1}{4}(u_z^+ + u^{+2}) + \frac{1}{W}\left[\frac{\phi}{(1+\phi_z^2)^{\frac{1}{2}}} - \frac{\phi^2\phi_{zz}}{(1+\phi_z^2)^{\frac{3}{2}}}\right]^+. \tag{2.17}$$

The elimination of q^+ between this result and (2.16) yields the following constraint which supplies the needed condition at $z = 0$:

$$\tfrac{1}{4}(u_z^+ + u^{+2}) = \frac{1}{W}\left[\frac{\phi}{(1+\phi_z^2)^{\frac{1}{2}}} + \frac{\phi^2\phi_{zz}}{(1+\phi_z^2)^{\frac{3}{2}}}\right]^+. \tag{2.18}$$

3. Nonlinear solution

In this section a single equation is obtained for determining the steady draw-down radius. Then a change of co-ordinates generates a system of equations that is convenient for numerical integration. Upon use of (2.9) we eliminate v from (2.10); then the result can be integrated once to yield

$$\left[\frac{1}{W(1+\phi_z^2)^{\frac{3}{2}}} - \frac{1}{4\phi^3}\right]\phi_{zz} - \frac{1}{W\phi(1+\phi_z^2)^{\frac{1}{2}}} + \frac{1}{4\phi^4}\phi_z^2 - \frac{1}{2\phi^4} = -\frac{z}{F} + C, \tag{3.1}$$

where C is the integration constant and is not to be confused with the integration constant in (2.15). In order to evaluate C we must evidently know ϕ, ϕ_z and ϕ_{zz} at some value of z.

It is not possible to integrate (3.1) again so numerical solutions are sought. An alternative form of this equation that is more convenient for numerical integration is obtained by a change of variables to arc length s in the axial direction along the jet surface, and angle θ as shown in figure 1, and represented by the transformation

$$z_s = \sin\theta, \quad \phi_s = \cos\theta, \tag{3.2}$$

so that

$$\phi_z = \cot\theta, \quad (1+\phi_z^2)^{-\frac{1}{2}} = \sin\theta, \quad \phi_{zz} = -\theta_s/\sin^3\theta. \tag{3.3}$$

In terms of these variables (3.1) appears as

$$\left(\frac{1}{W} - \frac{1}{4\phi^3\sin^3\theta}\right)\theta_s + \frac{1}{W\phi}\sin\theta + (\tfrac{1}{2} - \tfrac{1}{4}\cot^2\theta)\frac{1}{\phi^4} = \frac{z}{F} - C. \tag{3.4}$$

The integration constant C can be expressed in terms of the initial values

$$\theta_s(0) = \theta_s^0, \quad \theta(0) = \theta^0, \quad z(0) = 0, \quad \phi(0) = 1, \tag{3.5}$$

as

$$-C = \left(\frac{1}{W} - \frac{1}{4\sin^3\theta^0}\right)\theta_s^0 + \frac{1}{W}\sin\theta^0 + \tfrac{1}{2} - \tfrac{1}{4}\cot^2\theta^0. \tag{3.6}$$

If the initial values in (3.5) are known, C can be determined from (3.6). Then (3.2) and (3.4) represent a first-order system of three ordinary differential equations that can be integrated as an initial-value problem by standard numerical methods. However the initial values θ^0 and θ_s^0 are not known *a priori* for the problem at hand. Since some of the

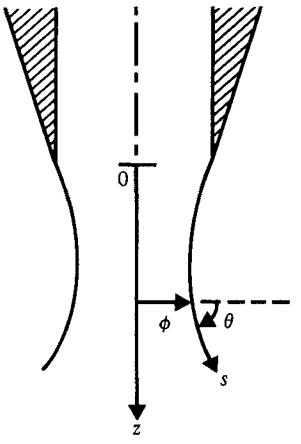

FIGURE 1. Jet configuration and co-ordinates ϕ = radius, z = axial co-ordinate, θ = angle of surface, s = arc length along surface in a plane containing jet axis.

boundary conditions of the problem are set at $z \to \infty$ in (2.12), it cannot be expected that both these conditions at $z = 0$ would be known. On the other hand the constraint (2.18) can be used to obtain one relation between θ^0 and θ_s^0. If use is made of (2.2), (2.9), (3.2) and (3.3) in (2.18) this condition yields

$$\theta_s^0 = \left(\frac{1}{W} - \frac{1}{4\sin^3\theta^0}\right)^{-1}\left(\frac{\sin\theta^0}{W} + \tfrac{1}{2}\cot^2\theta^0\right). \tag{3.7}$$

This condition along with (3.5) and the requirement $\phi \to 0$, $\theta_s \to 0$ as $s \to \infty$, are sufficient to determine the solution by numerical integration using a technique of interactive computing to be described in the next section.

4. Numerical integration of nonlinear equations – inviscid case

The procedure for integrating numerically the first-order system (3.2) and (3.4) as an initial-value problem evolved in the following manner. For prescribed values of W and F (or equivalently W and B), appearing in (3.4) a pair of values θ^0 and θ_s^0 were chosen as initial guesses. The numerical integration was carried out on a PDP-11/60 computer with graphical output. It was found that the resulting curve for ϕ *vs.* z usually diverged for small values of z. By keeping θ^0 fixed it was possible to guess different values of θ_s^0 and systematically improve the results. Figure 2 shows the curves for $W = 6$, $B = 0{\cdot}25$, $\theta^0 = 1{\cdot}753$ radians, and for various values of θ_s^0. As is apparent from figure 2 the integration is highly sensitive to the chosen value of θ_s^0. The solution of the problem at hand has the property that the curvature θ_s approaches zero monotonically (for downward-flowing jets) with s (or z) and becomes very small after about one jet diameter. When this happens equation (3.4) is no longer suitable for numerical integration. However, since θ_s is monotonic it can be assumed that once θ_s becomes very small it will remain very small. This observation led to a simple approximation procedure which appears to yield quite suitable results. First the numerical integration is carried out for various choices of θ_s^0 with all other parameters fixed until a suitable value of θ_s^0 is obtained. θ_s^0 is deemed suitable if the value of $|\theta_s|$ resulting from the

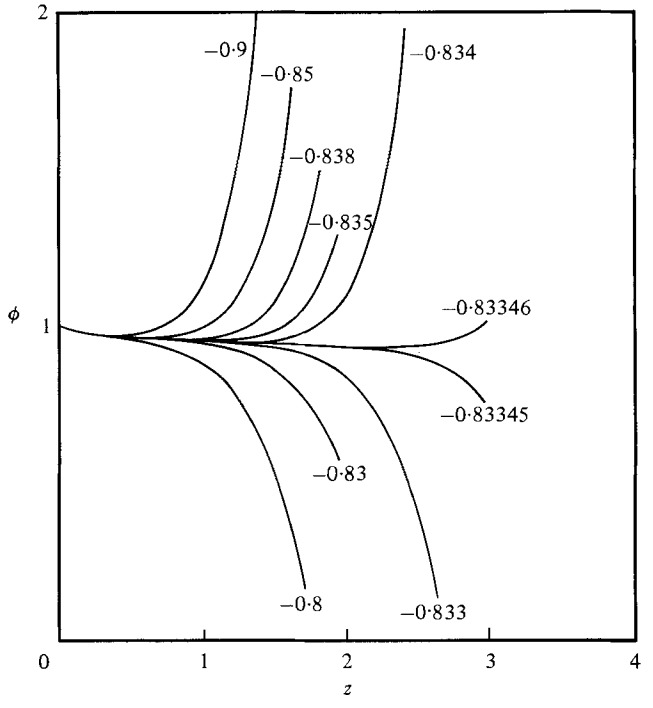

FIGURE 2. Jet radius ϕ *versus* axial distance z determined by the numerical integration of (3.2), (3.4) for $W = 6$, $B = 0{\cdot}25$, $\theta^0 = 1{\cdot}753$ and various values of θ_s^0.

corresponding numerical solution eventually becomes less than some chosen value $\varepsilon \ll 1$ (usually 10^{-3}). Suppose that

$$|\theta_s(s^*)| < \varepsilon, \quad \theta(s^*) = \theta^*, \quad \phi(s^*) = \phi^*, \quad z(s^*) = z^*. \tag{4.1}$$

Then since θ_s is monotonic (and negative),

$$|\theta_s(s)| < \varepsilon \quad \text{for} \quad s > s^*,$$

and we can set

$$\theta_s = 0, \quad \theta = \theta^* \quad \text{for} \quad s > s^* \tag{4.2}$$

in (3.4). After evaluating $C = C^*$ from (3.4) and (4.1) we obtain the following polynomial equation for determining ϕ for $z > z^*$,

$$\phi^4 - [\sin\theta^*/W(F^{-1}z - C^*)]\phi^3 - (2 - \cot^2\theta^*)/4(F^{-1}z - C^*) = 0. \tag{4.3}$$

This polynomial was solved numerically using standard library computer programs. The resulting solution is shown in figure 3 as the dashed curve for the parameters mentioned previously.

With W and B fixed the procedure just described determines a unique value of θ_s^0, and hence a solution, for a range of values of θ^0. Figure 4(a) shows (continuous curve) the values of θ_s^0 as a function of θ^0 for $W = 6$ and $B = 0{\cdot}25$. The points on this curve were determined by the method which resulted in figure 2 for values of θ^0 up to 2·52. For larger values of θ^0 the procedure did not yield a suitable value of θ_s^0. Also shown in figure 4(a) is the graph (dashed curve) for θ_s^0 determined by (3.7), which resulted from

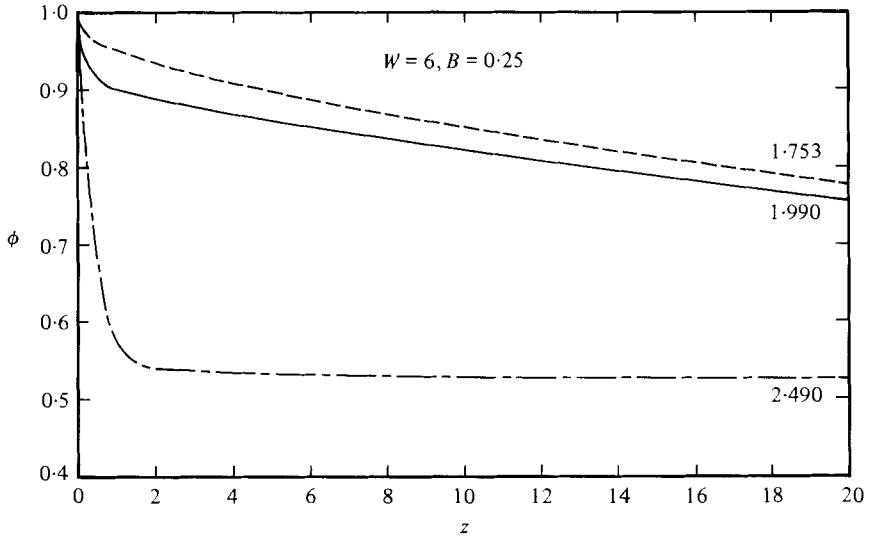

FIGURE 3. Jet radius ϕ *versus* axial distance z determined by the numerical integration of (3.2), (3.4) and (4.1)–(4.3) for $W = 6$, $B = 0{\cdot}25$ and three values of θ^0. Continuous curve ($\theta^0 = 1{\cdot}990$) represents the solution.

the constraint at $z = 0$. The two curves intersect in $\frac{1}{2}\pi < \theta^0 < \pi$ at two points, giving two different pairs θ^0, θ_s^0 for the initial slope and curvature. Both pairs satisfy the constraint (3.7) and integrate to a suitable set of values as given in (4.1). Therefore two possible solutions of the problem are determined for $W = 6$, and $B = 0{\cdot}25$. The 'small-angle' solution has $\theta^0 = 1{\cdot}990$, $\theta_s^0 = -1{\cdot}55$ and the 'large-angle' solution has $\theta^0 = 2{\cdot}490$, $\theta_s^0 = -0{\cdot}993$. Both of these solutions are also shown in figure 3. The small-angle solution is plotted with a continuous line while the large-angle solution is a dash–dot curve. Experimental observations, to be discussed in § 6, tend to support the occurrence of the small-angle and not the large-angle solution. The latter is evidently unstable. This hypothesis needs to be verified by a stability analysis, which is beyond the scope of the present investigation. It is assumed here that the small-angle solution is the only physically relevant one. Therefore the three shapes shown in figure 3 should be viewed as follows: the dashed curve is not a solution because the initial slope θ^0 and curvature θ_s^0 do not satisfy the constraint (3.7); the dashed–dot curve is the large-angle solution corresponding to the large-angle intersection in figure 4(a), and it is presumed to be unstable and therefore not physically relevant; the continuous curve is the small-angle solution corresponding to the small-angle intersection in figure 4(a), and it is presumed to be the solution of interest.

Figure 4(b) is similar to figure 4(a) except here $W = 4{\cdot}2$ and no intersection occurs. As W decreases the two points of intersection in figure 4(a) move closer together until a value $W_{\rm cr}$ is reached for which the two points coincide and the two curves are tangent at one point only. For $W > W_{\rm cr}$ there are no points of intersection of the two curves and therefore no steady solution is obtained satisfying the constraint (3.7). This occurs at $W \approx 4{\cdot}38$ for $B = 0{\cdot}25$.

Figure 5 shows by dashed lines the curves determined by the constraint (3.7) for various values of W in $2{\cdot}5 \leqslant W \leqslant \infty$. Also shown there by continuous lines are the

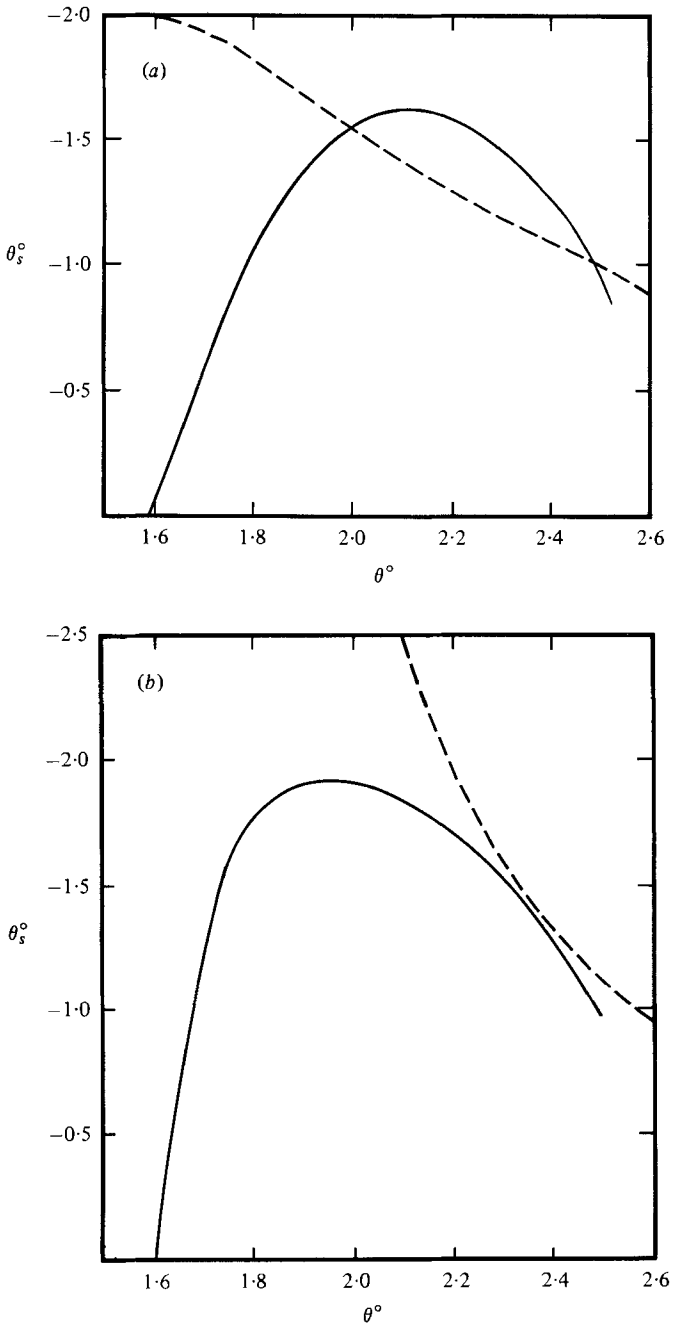

FIGURE 4. Initial curvature θ_s^0 versus initial angle θ^0. Continuous curve is determined from trial-and-error scheme depicted in figure 2 for various θ^0. Dashed curve is a plot of constraint equation (3.7). (*a*) Intersection points give initial conditions for possible solution, $W = 6$. (*b*) $W = 4{\cdot}2$. There is no intersection. $B = 0{\cdot}25$.

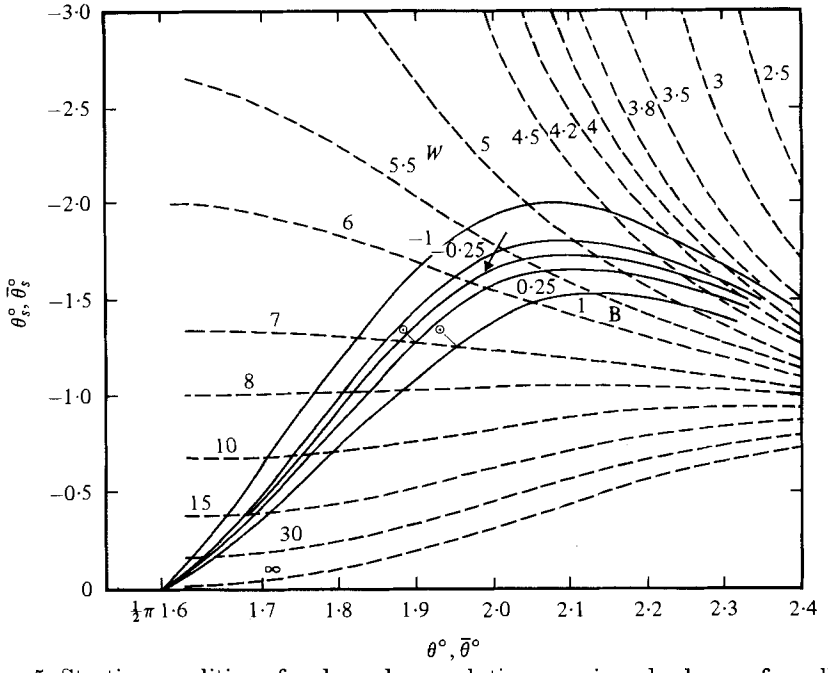

FIGURE 5. Starting conditions for draw-down solutions as given by locus of small-angle intersection points from curves shown in figure 4 for various values of W and B (solid lines). Dashed lines give plot of constraint equation (3.7) for various W.

loci of the unique small-angle pairs $\bar{\theta}^0$, $\bar{\theta}_s^0$ for various values of B in $-1 < B < 1$. All the points used for determining these curves were obtained by the intersection method illustrated in figure 4 (a). Thus, for each value of W, curves similar to those in figure 4 (a) were obtained and these curves determined one point of intersection which was then plotted in figure 5.

In summary, the procedure for obtaining the solution for given $W > W_{cr}$ and B is as follows:

(i) Use figure 5 to get the initial values $\bar{\theta}^0$, $\bar{\theta}_s^0$.

(ii) Calculate $\bar{C}$ from (3.6).

(iii) Numerically integrate (3.2) and (3.4) with

$$C = \bar{C}, \quad \theta_s^0 = \bar{\theta}_s^0, \quad \theta^0 = \bar{\theta}^0, \quad z^0 = 0, \quad \phi^0 = 1$$

until (4.1) is satisfied for chosen ε. Some adjustment of the value θ_s^0 will be necessary since the curves cannot be read with sufficient accuracy to ensure that (4.1) will be satisfied. (Recall figure 2.)

(iv) Calculate $C = C^*$ from (3.4) with (4.2).

(v) Solve the polynomial (4.3) for ϕ when $z > z^*$.

Figure 6 shows the radius ϕ as a function of z for several values of the Weber number W with the Bond number $B = 0{\cdot}25$. The Bond number is fixed by the choice of nozzle and fluid, whereas the Weber number varies with initial velocity v_0. Therefore the sequence shown in figure 6 is for a chosen nozzle and fluid with various initial velocities. At high velocity ($W = 1000$) the profile is almost straight, whereas for low velocity ($W = 4{\cdot}5$) there is severe draw-down near the nozzle. In an experiment where the nozzle velocity is gradually reduced, B remains fixed while W decreases. According to the solution presented here the drawn-down profile passes through a sequence of

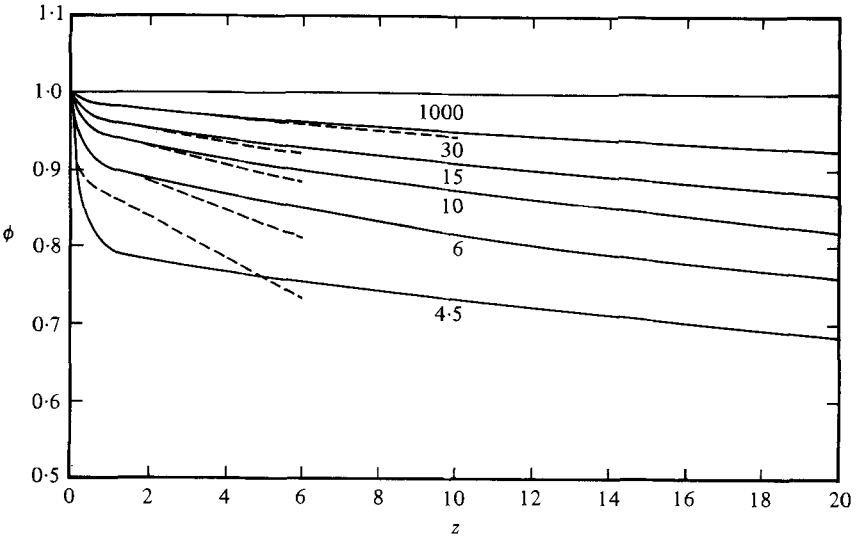

FIGURE 6. Jet radius ϕ *versus* axial distance z for $B = 0{\cdot}25$ and various values of W. Continuous line gives nonlinear solution determined by numerical integration. Dashed line gives solution from linear theory (5.2), (5.9), (5.12), (5.18).

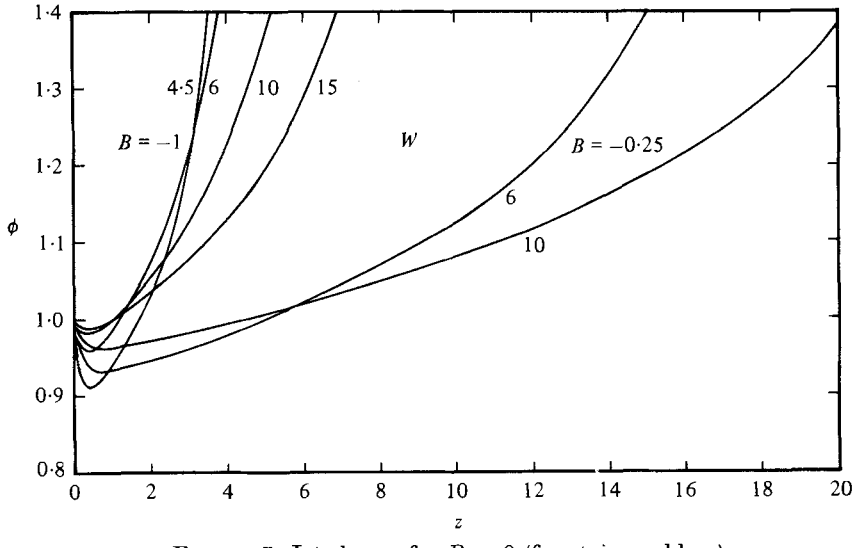

FIGURE 7. Jet shapes for $B < 0$ (fountain problem).

shapes shown in figure 6 (for $B = 0{\cdot}25$) until W reaches W_{cr}. For $W < W_{cr}$ no steady drawn-down solution is obtained. In §6 experiments will be discussed that suggest W_{cr} determines the 'cut-off' condition for transition from a steady draw-down to a non-steady drip from the nozzle.

The profiles in figure 6 have the property that the maximum curvature occurs at $z = 0$ for points on the continuous curves in figure 5 to the left of their maxima. For $B = 0{\cdot}25$ these points correspond to $W > 5{\cdot}4$. If $W < 5{\cdot}4$ the maximum curvature is not at $z = 0$ but occurs a short distance downstream from $z = 0$. Therefore in these

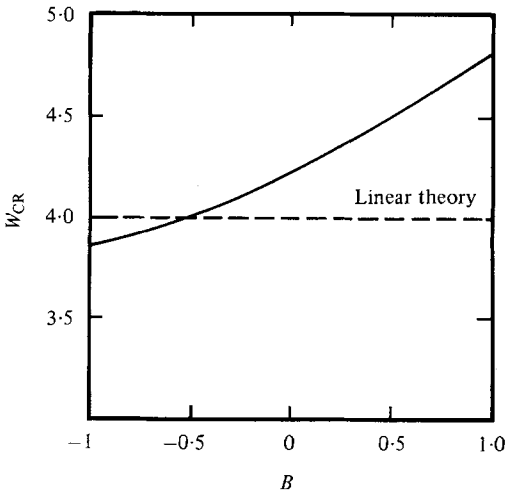

FIGURE 8. Cut-off Weber number, W_{cr}, versus Bond number B. Continuous curve is from nonlinear theory; dashed curve is for linear theory.

cases θ_s is not monotonic but passes through one extremum and then monotonically approaches zero.

Figure 7 shows profiles for $B < 0$, i.e. for the fountain problem. Here the curvature θ_s integrates to small values as for $B > 0$, but farther down the jet the curvature again increases as the jet velocity decreases due to gravity. The procedure for computing these profiles is the same as for $B > 0$. The diverging radius is predicted by the polynomial in (4.3) and this procedure rests on the assumption that θ_s remains small, which is questionable here. Nevertheless the results appear to be qualitatively correct and are numerically correct for $z < 1{\cdot}5$ where the integration scheme was used.

Finally figure 8 shows the dependence of W_{cr} on B. The continuous curves in figure 5 for fixed B terminate at the appropriate value of W_{cr} and for $\bar{\theta}^0$ in the range

$$2{\cdot}3 < \bar{\theta}^0 < 2{\cdot}4.$$

5. Linear analysis

Assume

$$\phi_z(0) = -\epsilon, \quad \epsilon \ll 1, \tag{5.1}$$

and linearize (2.9) and (2.10) by the expansions

$$\phi = 1 + \epsilon\phi_1 + \ldots, \quad v = 1 + \epsilon v_1 + \ldots \tag{5.2}$$

and with the added assumption

$$\frac{z}{F} = \epsilon G z = O(\epsilon). \tag{5.3}$$

The resulting linear equations for ϕ_1 and v_1 are

$$2\phi_1 + v_1 = 0, \tag{5.4}$$

$$v_{1z} - \tfrac{1}{8}v_{1zzz} - \frac{1}{W}(\phi_{1z} + \phi_{1zzz}) = G. \tag{5.5}$$

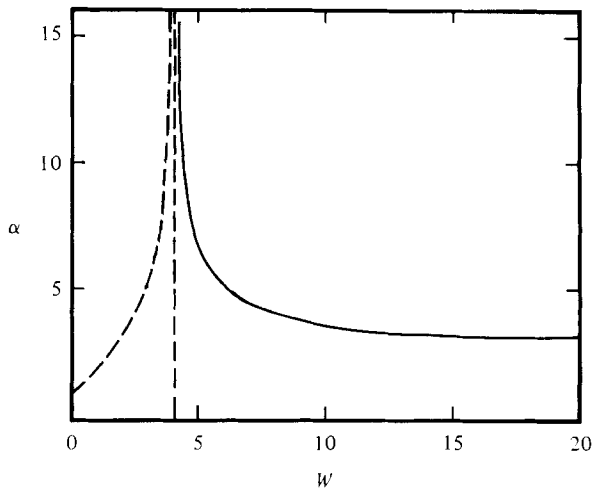

FIGURE 9. Linear theory α versus W from (5.9) for inviscid case (dashed curve is $|\alpha|$ for imaginary α when $W < 4$).

Also the boundary conditions (2.11) become

$$\phi_1(0) = v_1(0) = 0, \tag{5.6}$$

and (5.1) produces the additional condition

$$\phi_{1z}(0) = -1. \tag{5.7}$$

With the use of (5.4) v_1 can be eliminated in (5.5) and there results after one integration

$$\phi_{1zz} - \alpha^2\phi_1 = \frac{4W}{W-4}Gz + C, \tag{5.8}$$

where C is the constant of integration and

$$\alpha^2 = 4(1+2W)/(W-4). \tag{5.9}$$

Observe that $\alpha^2 > 0$ if $W > 4$, $\alpha^2 < 0$ if $W < 4$ and α^2 is undefined for $W = 4$. Figure 9 shows α *vs.* W for $W > 4$ and $\bar{\alpha} = |\alpha|$ *vs.* W for $W < 4$.

Solution for $W > 4$. The general solution of (5.8) for $\alpha^2 > 0$ is

$$\phi_1 = A\,e^{-\alpha z} + D\,e^{\alpha z} - \frac{WG}{1+2W}z + C', \tag{5.10}$$

where A and D are arbitrary constants and C' is an integration constant different from C. If ϕ_1 is to remain bounded for large z we must take $D = 0$. Then (5.6) with (5.10) yields

$$\phi_1 = A(e^{-\alpha z} - 1) - \frac{WG}{1+2W}z, \tag{5.11}$$

and (5.7) determines A so that

$$\phi_1 = \frac{1}{\alpha}\left(1 - \frac{WG}{1+2W}\right)(e^{-\alpha z} - 1) - \frac{WG}{1+2W}z. \tag{5.12}$$

In order to use this result with (5.2) and (5.3) to determine the drawn-down jet

shape we must first specify the value of ϵ in (5.1), which represents the initial slope of the profile. This we obtain from the linearized form of the constraint (3.7). From (3.3) and (5.1) there results

$$\epsilon = -\cot\bar{\theta}^0. \tag{5.13}$$

If $\gamma \ll 1$ is defined by

$$\bar{\theta}^0 = \tfrac{1}{2}\pi + \gamma \tag{5.14}$$

then

$$\epsilon = \tan\gamma \simeq \gamma. \tag{5.15}$$

Next, the linearization of (3.7) and (3.3), with (5.1), yields

$$\bar{\theta}^0_s = \frac{4}{4-W} = -\phi_{zz}(0) = -\epsilon\phi_{1zz}(0). \tag{5.16}$$

Now return to (5.12) to obtain with (5.3)

$$\phi_{1zz}(0) = \alpha\left(1 - \frac{W/F}{1+2W}\frac{1}{\epsilon}\right). \tag{5.17}$$

Finally (5.16), (5.17) and (5.9), (2.8) yield the following expression for ϵ:

$$\epsilon = \frac{B}{1+2W} + \frac{2}{[(1+2W)(W-4)]^{\frac{1}{2}}}. \tag{5.18}$$

Observe that $\epsilon \ll 1$ only if W is much greater than 4 and $B/W = F^{-1}$ is small. Therefore the linear analysis is reliable only for

$$W = \rho a v_0^2/\sigma \gg 4 \quad \text{and} \quad B/W = v_0^2/ga \gg 1. \tag{5.19}$$

We also observe from (5.18) that $\epsilon \to 0$ in the limit $W \to \infty$, which, in view of (5.11), means that (2.16) implies $\phi_z^+ = 0$ in the high-velocity limit as would be expected. The values of $\bar{\theta}^0$ determined by (5.14), (5.15) and (5.18), and $\bar{\theta}^0_s$ determined by (5.16) can be compared with the corresponding quantities of the nonlinear analysis plotted in figure 5. The values $4/(4-W)$ agree with the dashed curves at $\theta^0 = \frac{1}{2}\pi$ and these values are seen to be reasonable approximations of $\bar{\theta}^0_s$ for $W > 7$ when B is also small. The two circled dots on figure 5 are the linear theory pairs of $\bar{\theta}^0$, $\bar{\theta}^0_s$ for $W = 7$ and $B = 0{\cdot}25$ and 1. The thin lines connect these points to the corresponding points of the nonlinear analysis. This illustrates that both conditions in (5.19) need to be satisfied in order for the linear theory to give a good approximation.

In summary, the linearized analysis gives $\phi = 1 + \epsilon\phi_1$, where ϵ is determined in terms of B and W from (5.18), ϕ_1 is given by (5.12) in which $G = (\epsilon F)^{-1}$ and α is given by (5.9). The linear analysis is reliable only when (5.19) are satisfied, and then only for a range of z such that (5.3) is satisfied. Drawn-down shapes were calculated for $B = 0{\cdot}25$ and various values of W, and the results are plotted as dashed lines in figure 6 alongside the corresponding curves obtained from the nonlinear analysis. The comparison shows that the linearized theory gives good results for $W = 30$ for values of z up to 10. As W decreases the range of z for good agreement decreases. At $W = 10$ agreement is good for $z < 2$ and at $W = 6$ the agreement is good for $z < 1{\cdot}5$. The value of ϵ is 0·411 for this case. Surprisingly the result is not as bad as expected for $W = 4{\cdot}5$ although reasonable agreement occurs only for $z < 0{\cdot}2$. In this case the value of ϵ is 0·919.

The above procedure yields a solution of the type just described for all values of

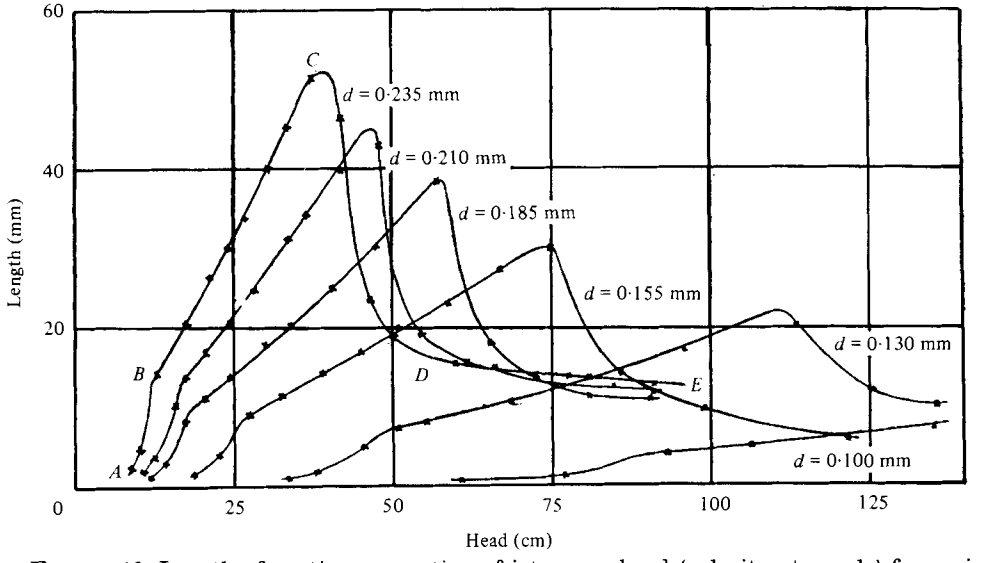

FIGURE 10. Length of continuous portion of jet *versus* head (velocity at nozzle) for various nozzle diameters. Experimental results reproduced from Smith & Moss (1917).

$W > 4$. As $W \to 4$ both α and ϵ become unbounded. For $W < 4$ α is imaginary so the solution (5.10) is oscillatory. Then the constant D in (5.10) is not required to be zero by a boundedness condition, and so another boundary condition would be required for the solution. We therefore conclude that the linear theory predicts $W_{cr} = 4$ as compared to figure 8 for the nonlinear solution.

6. Comparison with experiments

The first extensive experimental observations for the steady draw-down of a liquid jet emanating from a nozzle were reported by Smith & Moss (1917). They focused on the length of the continuous portion between the nozzle and the point of drop formation, and they measured this 'jet length' as a function of 'head' (or velocity at the nozzle). Figure 10 (from Smith & Moss) shows their unreduced results for a mercury jet discharging into a solution of mercurous nitrate for various size glass nozzles. Quoting them:

> Considering the curve *ABCDE*, of this figure,... it will be seen that between *A* and *B*, where the heads are at first only just sufficient to cause the jet to form, the jet-length increases very rapidly, as the head rises. At *B* the rate of increase of l with h changes suddenly, becoming smaller and remaining practically constant till *C* is reached. Beyond this point the jet-length falls very rapidly at first, as the head is increased. At the higher head (near *E*) the rate of decrease of jet-length is comparatively small. Between *C* and *D* the jet is relatively unstable, lengthening and shortening in a capricious way which makes definite measurement of its length difficult...

Similar results were obtained with other fluids and the points *B* and *C* were designated as first and second 'critical points' of the curve. By varying surface tension and

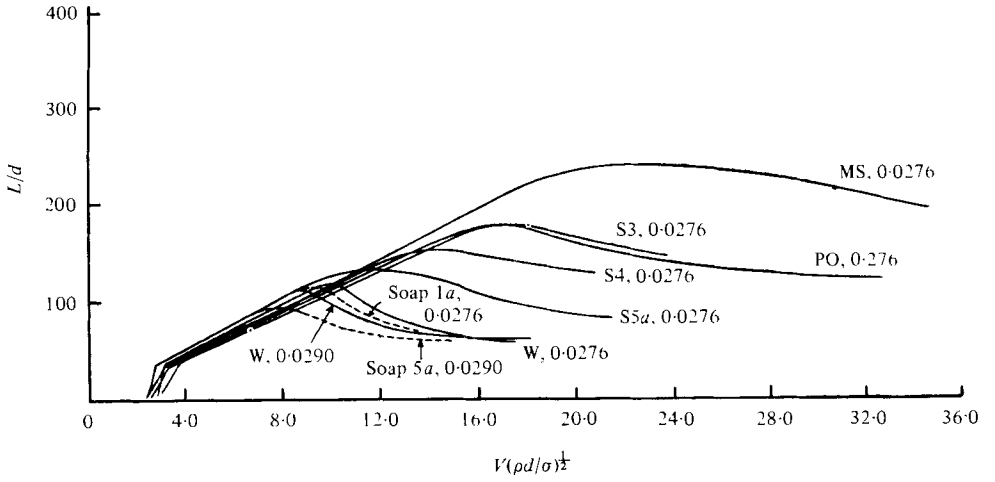

FIGURE 11. Dimensionless length of continuous portion of jet *versus* $V(\rho d/\sigma)^{\frac{1}{2}}$ (V = velocity, ρ = density, d = diameter, σ = surface tension) for various nozzle diameters and liquids. Experimental results reproduced from Tyler & Richardson (1925). W, water; MS, methylated spirits; PO, paraffin oil; S3, S4, S5*a*, sugar – the number refers to table 1; – – – –, Soap 1*a*, Soap 5*a*, soap solutions. The values of d are also shown on the figure. Table 1 contains further information concerning the experiments.

viscosity Smith & Moss determined that region A–C is controlled by surface tension while C–E is controlled primarily by viscosity. The second critical point C coincides with the onset of turbulence. They also found that the results depend 'appreciably upon the form of the nozzle'.

A formula describing the length of the jet was derived by Smith & Moss on the basis of Rayleigh's (1879) stability theory. From this relation it was observed that the segment between A and B 'can be accounted for if we assume . . . the initial amplitude of the disturbance decreases at first as the velocity of efflux rises'. When the experimental results were plotted as l/d *vs.* $V/(\rho d/\sigma)^{\frac{1}{2}}$ (d = diameter, V = velocity, ρ = density, σ = surface tension) the segment between B and C was found to be a straight line, which if extended would pass through the origin. Furthermore, this line and point B were essentially the same for all the different fluids and nozzles. This is demonstrated by figure 11 and table 1 reproduced here from Tyler & Richardson (1925), who continued and expanded the experiments of Smith & Moss. Here the first and second critical velocities are designated V_1 and V_2 respectively. The Weber number W defined in (2.6) is related to $V(\rho d/\sigma)^{\frac{1}{2}}$ in figure 11 by

$$W = \tfrac{1}{2}(V(\rho d/\sigma)^{\frac{1}{2}})^2.$$

The values of W associated with the column $V_1(\rho d/\sigma)^{\frac{1}{2}}$ range from 3·70 to 5·51 if the lowest and highest values (which correspond to the first two results for methylated spirit) are excluded. The average of these values is 4·69. The values of B, defined in (2.8), range between 0·01 and 0·03 for the results in figure 11. For B in this range, the critical Weber number below which a steady solution was not obtained is given in figure 8 as $W_{cr} \simeq 4{\cdot}25$. The suggestion is, therefore, that the experimentally observed first critical velocity is associated with the W_{cr} derived here. This view is supported

Liquid	d (cm)	Temperature (° C)	σ (dynes cm^{-1})	ρ (g cm^{-3})	V_1 (cm s^{-1})	V_2 (cm s^{-1})	$V_1\left(\frac{\rho d}{\sigma}\right)^{\frac{1}{2}}$	$V_2\left(\frac{\rho d}{\sigma}\right)^{\frac{1}{2}}$	$\frac{\mu}{(\sigma\rho d)^{\frac{1}{2}}}\times 10^4$
Water	0·0290	17	72·3	1·00	139	437	2·79	8·77	74·7
	0·0276	15	70·5	1·00	160	490	3·16	9·7	81·9
Paraffin	0·0550	20	26·4	0·804	—	340	—	13·9	140·5
	0·0276	20	26·4	0·804	110	590	3·19	17·15	199·0
1	0·0276	15	71·0	1·017	160	502	3·16	10·0	88·5
2	0·0276	18	71·7	1·055	162	549	3·20	10·9	107·8
3	0·0276	18	71·8	1·120	160	825	3·32	17·2	180·3
4	0·0276	16	72·7	1·085	160	711	3·25	14·4	141·0
Sugar solution 1*a*	0·0290	17	73·9	1·090	140	710	2·90	14·70	141·0
2*a*	0·0290	14	73·3	1·135	150	1000	3·18	21·21	232·0
3*a*	0·0290	16	73·3	1·098	140	740	2·91	15·40	155·0
4*a*	0·0290	16	73·0	1·115	130	841	2·72	17·62	178·5
5*a*	0·0290	16	72·3	1·053	140	557	2·86	11·45	101·6
Methylated spirits	0·0276	17	23·7	0·813	118	727	3·65	22·47	250·0
Methylated spirits–water	0·0276	18	53·0	0·95	105	767	2·3	17·15	180·5
	0·0276	15	43·2	0·98	130	753	3·2	18·80	210·0
Soap solution	0·0550	19	—	0·99	—	250	—	6·9†	50·0†
	0·0276	15	—	0·99	—	470	—	9·3	81·9
	0·0290	15	—	0·99	140	400	—	8·32	69·8

† Assuming $\sigma = 73$ dynes cm^{-1}.

TABLE 1

by the statement in Tyler & Richardson, p. 309, where it is observed that, in the region below the first critical velocity, 'the continuous portion of the jet is traversed by ripples'. Such observable ripples would mean that the solution is not steady.

A simple experiment was conducted to check the above hypothesis of unsteady flow below the first critical velocity. A 5-gallon bottle was fitted with a rubber stopper in which three holes were drilled. One hole held securely a 1·2 mm internal diameter glass capillary nozzle. The other two holes carried glass tubes that reached nearly to the bottom of the jar on the inside and protruded enough on the outside for flexible hoses to be attached. One of these hoses was connected to a U-tube manometer containing water, and the other was fitted with a valve for adjusting the rate of air flow into the bottle after a partial vacuum was created by the discharge of some of the water. The entire bottle assembly was secured in a frame that was hinged on a horizontal axis so the bottle could be turned from the nozzle-up to the nozzle-down position. As the water discharged the bottle pressure gradually reduced and the length of the jet shortened until the first critical point was reached. Below this point the inlet air valve had to be carefully adjusted to keep the continuous portion from disappearing altogether. When this was done the ripples mentioned by Tyler & Richardson were indeed observed at times and this observation tends to confirm that the portion of the curves below the first critical point is associated with unsteady flow.

7. Discussion of the solution and its limitations

The solution obtained here for steady draw-down and cut-off of an inviscid liquid jet under surface tension and gravity is based on a one-dimensional theory that has previously been used to solve other jet problems. The formulation of the problem sets some of the conditions far downstream from the nozzle and they cannot all be incorporated into the solution method, which is numerical integration of ordinary differential equations as an initial-value problem. Insufficient initial conditions are known at the nozzle but a constraint between the initial slope and initial curvature is obtained at the nozzle and this determines the solution for the inviscid jet. This constraint is a direct result of evaluating the integration constant in (2.13) according to (2.15). Attempts to prove that C must take this value have not been successful and a different choice for C would lead to a different constraint. Because of our interest in the low-velocity range the condition valid for zero velocity static pendant drops was studied and found to be the same as (2.16). However, the linear analysis in §5 indicates that this choice also gives the proper condition in the high-velocity limit.

The solution gives draw-down shapes for prescribed values of W and B as defined in (2.6) and (2.8) for values of $W > W_{cr}$, where W_{cr} is shown as a function of B in figure 8. For $W < W_{cr}$ no steady solution is obtained.

The linearized equations yield a simple solution which is compared with the non-linear solution in figure 6. The approximation of the linear theory is reasonable for a short length of the jet for $W > 7$ and $B \simeq 0$. The linear theory predicts $W_{cr} = 4$ for the inviscid jet which is also a good approximation to W_{cr} given in figure 8. This correspondence lends credibility to the constraint condition discussed above, since W_{cr} in the nonlinear theory is associated with the constraint while W_{cr} in the linearized theory results directly from (5.9).

Experiments were cited which indicate that a critical value of W occurs near $W = 4{\cdot}5$.

Below this critical value the jet is not steady in the continuous portion, in agreement with the predictions of the solution. Of course the steady solution for $W > W_{cr}$ is also not stable and breaks up according to Rayleigh's theory, but a steady solution exists. For $W < W_{cr}$ no steady solution is found and experiments reveal observable ripples on the continuous portion of the jet.

When $W = 0$ a steady solution exists for low enough nozzle pressure and it is the static pendant drop solution. As pressure increases and the volume of the drop increases this solution becomes unstable and the drop detaches (see Pitts 1974). As W increases from $W = 0$ the jet first drips at the nozzle, which means that the angle θ^0 of the meniscus at the nozzle is time dependent and varies between two values θ_1^0 and θ_2^0, say. Then as W increases more the supply is too great for distinct drops to form at the nozzle so a continuous length occurs that still has time-dependent θ^0. This relatively large disturbance at the nozzle causes break-off at a very short length. This prevails until W reaches W_{cr}. Then the steady solution exists and the disturbance at the nozzle is much smaller, accounting for the discontinuity in the experimental curves at the 'first critical point'.

Of course, the inviscid solution obtained here cannot account for any effects associated with the change in velocity profile that occurs just outside the nozzle. For example, the profile could be that of Poiseuille flow inside the nozzle and it becomes essentially uniform a few diameters downstream from the nozzle. For a viscous fluid these effects are known to be important, and in some cases they may dominate. See Middleman & Gavis (1961), where highly viscous Newtonian jets are found to expand rather than contract as they emerge from the nozzle.

This work was partially supported by the IBM Research Laboratory in San Jose, California. The numerical integration was carried out on the PDP-11/60 minicomputer of the Department of Mechanical Engineering, University of California, Berkeley, using the PARASOL program written by Professor D. Auslander. The author is indebted to the reviewers for several helpful suggestions.

REFERENCES

Bogy, D. B. 1978 *Phys. Fluids* **21**, 190–197.

Bogy, D. B. 1979*a* *Phys. Fluids* **22**, 224–230.

Bogy, D. B. 1979*b* *Ann. Rev. Fluid Mech.* **11**, 207–228.

Caulk, D. A. & Naghdi, P. M. 1979*a* *Arch. Rat. Mech. Anal.* **69**, 1–30.

Caulk, D. A. & Naghdi, P. M. 1979*b* *J. Appl. Mech.* **46**, 291–297.

Duda, J. L. & Vrentas, J. S. 1967 *Chem. Eng. Sci.* **22**, 855–869.

Goren, S. L. & Wronski, S. 1966 *J. Fluid Mech.* **25**, 185–198.

Green, A. E. 1976 *Int. J. Engng Sci.* **14**, 49–63.

Green, A. E., Naghdi, P. M. & Wenner, M. L. 1974 *Proc. Roy. Soc.* A **337**, 485–507.

Harmon, D. B. 1955 *J. Franklin Inst.* **259**, 519–522.

Lienhard, J. H. 1968 *Trans. A.S.M.E.* D, *J. Basic Engng* **90**, 262–268.

Middleman, S., & Gavis, J. 1961 *Phys. Fluids* **4**, 355–359.

Naghdi, P. M. 1979 Proc. IUTAM Symp. on Non-Newtonian Fluid Mech. *J. Non-Newtonian Fluid Mech.* **5**, 233–265.

Pitts, E. 1974 *J. Fluid Mech.* **63**, 487–508.

Rayleigh, Lord 1879 *Proc. London Math. Soc.* **10**, 4–13.

Savart, F. 1833 *Ann. de Chim.* **53**, 337–386.

Scheele, G. F. & Meister, B. J. 1968 *A.I.Ch.E. J.* **14**, 15–19.
Scriven, L. E. & Pigford, R. L. 1959 *A.I.Ch.E. J.* **5**, 397–402.
Smith, S. W. J. & Moss, H. 1917 *Proc. Roy. Soc.* A **93**, 373–393.
Tyler, E. & Richardson, E. T. 1925 *Proc. Phys. Soc. London* **37**, 297–311.